

Lattice Distortion and Magnetic Quantum Phase Transition in $\text{CeFeAs}_{1-x}\text{P}_x\text{O}$

Clarina de la Cruz,^{1,2} W. Z. Hu,³ Shiliang Li,^{1,3} Q. Huang,⁴ J. W. Lynn,⁴ M. A. Green,⁴ G. F. Chen,^{3,5} N. L. Wang,³
H. A. Mook,² Qimiao Si,⁶ and Pengcheng Dai^{1,2,3,*}

¹*Department of Physics and Astronomy, The University of Tennessee, Knoxville, Tennessee 37996-1200, USA*

²*Neutron Scattering Science Division, Oak Ridge National Laboratory, Oak Ridge, Tennessee 37831, USA*

³*Institute of Physics, Chinese Academy of Sciences, Beijing 100190, China*

⁴*NIST Center for Neutron Research, National Institute of Standards and Technology, Gaithersburg, Maryland 20899-6012, USA*

⁵*Department of Physics, Renmin University of China, Beijing 100872, China*

⁶*Department of Physics and Astronomy, Rice University, Houston, Texas 77005, USA*

(Received 19 October 2009; published 8 January 2010)

We use neutron diffraction to study the structural and magnetic phase diagram of $\text{CeFeAs}_{1-x}\text{P}_x\text{O}$. We find that replacing the larger arsenic with smaller phosphorus in $\text{CeFeAs}_{1-x}\text{P}_x\text{O}$ simultaneously suppresses the AFM order and orthorhombic distortion near $x = 0.4$, thus suggesting the presence of a magnetic quantum critical point. Our detailed structural analysis reveals that the pnictogen height is an important controlling parameter for their electronic and magnetic properties, and may play an important role in electron pairing and superconductivity of these materials.

DOI: 10.1103/PhysRevLett.104.017204

PACS numbers: 75.30.Fv, 75.25.-j, 75.50.Ee

The discovery of ubiquitous antiferromagnetic (AFM) order in the parent compounds of iron arsenide superconductors [1–6] has renewed interest in understanding the interplay between magnetism and high-transition temperature (high- T_c) superconductivity in these materials [7–10]. Although superconductivity in iron arsenides can be induced either via charge carrier doping [1–3] or application of pressure [11] to their semimetal parent compounds, the resulting electronic phase diagrams are dramatically materials dependent, ranging from first-order-like AFM to superconductivity phase transition for $\text{LaFeAsO}_{1-x}\text{F}_x$ [12], to the gradual suppression of the AFM order before superconductivity for $\text{CeFeAsO}_{1-x}\text{F}_x$ [13], and finally to the coexisting AFM order with superconductivity in $\text{SmFeAsO}_{1-x}\text{F}_x$ [14]. Similar to the considerations made for the copper oxides [15], these properties make it possible that superconductivity is being influenced by a magnetic quantum critical point (QCP) located in the not-yet-accessed part of the overall phase diagram. To determine if iron arsenides indeed have a magnetic QCP, it is important to isoelectronically tune the crystal lattice structure without the influence of charge carrier doping and superconductivity [16]. In this Letter, we use neutron scattering to show that replacing the larger arsenic with smaller phosphorus in $\text{CeFeAs}_{1-x}\text{P}_x\text{O}$ simultaneously suppresses the AFM order and orthorhombic distortion near $x = 0.4$, providing evidence for a magnetic QCP. Furthermore, we find that the pnictogen height is an important controlling parameter for their electronic and magnetic properties, and may play an important role in electron pairing and superconductivity [17,18].

In the undoped state, the parent compounds of iron arsenide superconductors such as LaFeAsO [4] and CeFeAsO [13] have an orthorhombic lattice distortion and collinear AFM structure as shown in Figs. 1(a) and 1(b). The dis-

appearance of the static AFM order in superconducting samples [4] naturally raises the possibility of carrier-doping-induced quantum phase transitions, where quantum critical fluctuations at finite energies can influence transport properties and drive electron pairing for superconductivity [19]. Although carrier doping [1–3] or application of pressure [20] can reduce the AFM order and orthorhombic lattice distortion, the resulting electronic phase diagrams are dramatically materials dependent [12–14] with no strong evidence for the existence of a magnetic QCP. Applying a magnetic field to suppress the influence of superconductivity is a common means to unmask any potential quantum critical point [21], but this approach is difficult to implement here because of the large superconducting critical field for the iron pnictides [22]. We instead achieve the same purpose by isoelectronic phosphorus substitution for arsenic in CeFeAsO [16], recognizing that superconductivity appears neither in CeFeAsO , an antiferromagnet with orthorhombic lattice distortion [13], nor in CeFePO , a paramagnet with a tetragonal structure [23]. Our systematic neutron scattering studies of the structural and magnetic phase transitions in $\text{CeFeAs}_{1-x}\text{P}_x\text{O}$ demonstrate that the pnictogen height [the average Fe-As(P) distance] and orthorhombicity of the CeFeAs(P)O unit cell critically control the iron AFM ordered moment and Néel temperature [Figs. 1(c)–1(f)] of the system. These results are dramatically different from carrier-doping [1–3] and pressure-induced [11] AFM moment reduction, where the Fe-As distance and pnictogen height do not decrease with increasing doping [13] or pressure [20]. The experimental exposition of a magnetic QCP from our measurements, as well as recent transport studies on the same system [24], suggest the importance of collective magnetic quantum fluctuations to the overall phase diagram of the iron pnictides and, by extension, to

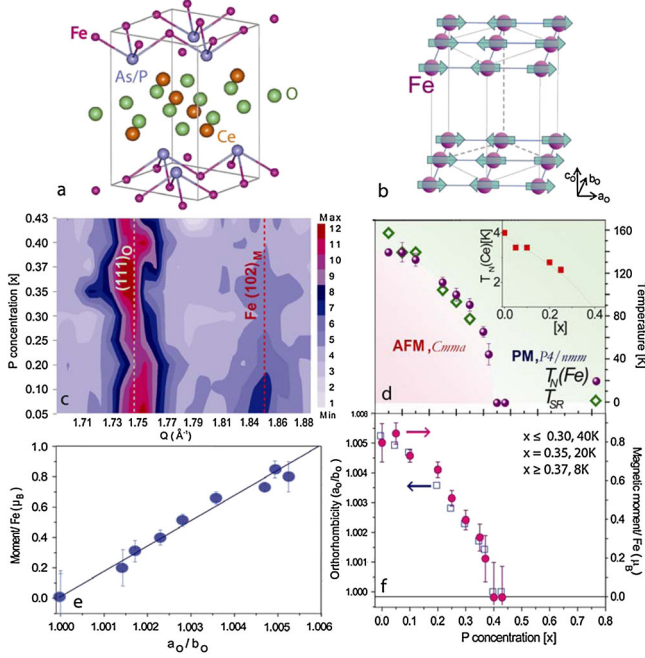


FIG. 1 (color online). (a) The three dimensional crystal lattice structure of CeFeAsO. (b) The magnetic unit cell of Fe in CeFeAsO. The Fe moments lie in the a - b plane and form an antiferromagnetic collinear structure similar to that of LaFeAsO [4], while nearest-neighbor spins along the c axis are parallel and so there is no need to double the magnetic cell along the c axis [13]. (c) Magnetic scattering at the Fe $(1, 0, 2)_M$ peak, normalized to the nuclear Bragg peak $(1, 1, 1)_O$. The vanishing magnetic peak intensity is clearly seen near $x \sim 0.4$. (d) Experimentally obtained structural and magnetic phase transition temperatures as a function of P substitution of As. The inset in (d) shows the P dependence of the Ce AFM ordering temperatures. (e) The ordered AFM moment of Fe is proportional to the orthorhombicity (defined as a_o/b_o) of the system and becomes zero at $a_o/b_o = 1$ (f) P-doping dependence of the orthorhombicity and Fe ordered moments. The Fe ordering temperatures are noted in the inset.

both the electronic properties in the normal state and the origin of superconductivity [18].

We prepared polycrystalline samples of CeFeAs $_{1-x}$ P $_x$ O with $x = 0.05, 0.10, 0.20, 0.25, 0.30, 0.35, 0.37, 0.40, 0.43$ using the method similar to CeFeAsO $_{1-x}$ F $_x$ [25]. The resistivity and ac susceptibility measurements carried out on these samples using a commercial physical property measurement system confirmed the absence of superconductivity above $T = 1.8$ K. In previous work, it was found that CeFeAsO undergoes the tetragonal (space group $P4/nmm$) to orthorhombic (space group $Cmma$) structural transition below ~ 158 K followed by a long-range commensurate AFM order below ~ 135 K [Figs. 1(a) and 1(b), Ref. [13]]. Similar to the electron doping of CeFeAsO via fluorine substitution of oxygen, we find that phosphorus replacement of arsenic on CeFeAsO also results in decreasing the structural and magnetic phase transition temperatures although here no charge carriers are doped into the FeAs layer [Fig. 1(d)]. Within experimental accuracy, we

cannot separate the structural from the magnetic phase transition for $x \geq 0.05$. In the limit of the low-temperature tetragonal structure ($a_o/b_o \rightarrow 1$) near $x \approx 0.4$, the static long-range ordered moment vanishes [Fig. 1(e)] and the system becomes tetragonal paramagnetic like CeFePO [23]. Figure 1(f) plots the phosphorus doping dependence of the orthorhombicity (a_o/b_o) and Fe ordered moment at low temperature. The smooth linear decrease of the ordered moment that tracks the distortion suggests the presence of a lattice-distortion-induced magnetic quantum phase transition through phosphorus doping. Although similar measurements have not been carried out on the electron-doped material such as BaFe $_{2-x}$ Co $_x$ As $_2$, the temperature dependence of the lattice distortion versus ordered magnetic moment in SrFe $_2$ As $_2$ showed identical linear behavior [26], thus suggesting that a direct coupling between the structural distortion and magnetism is a general phenomenon in iron arsenides.

To illustrate how the phase diagram in Fig. 1(f) is established, we show in Fig. 1(c) the phosphorus doping dependence of the nuclear $(1, 1, 1)_O$ and magnetic $(1, 0, 2)_M$ Bragg peaks (orthorhombic indexing) obtained using triple-axis spectrometers (TAS). The $(1, 0, 2)_M$ magnetic peak was chosen because its structure factor has no contribution from the Ce moment. Similar to CeFeAsO $_{1-x}$ F $_x$ [13], we find that phosphorus substitution of arsenic only suppresses the Fe ordered moment and does not change the commensurate magnetic ordering wave vector [Fig. 1(c)]. The suppression of the $(1, 0, 2)_M$ magnetic scattering relative to the nuclear $(1, 1, 1)_O$ peak is seen near $x \approx 0.4$, suggesting the presence of a magnetic quantum phase transition. For comparison, electron doping via fluorine substitution of oxygen suppresses the static AFM ordered moments more efficiently, near $x \approx 0.04$ and 0.06 for LaFeAsO $_{1-x}$ F $_x$ [12] and CeFeAsO $_{1-x}$ F $_x$ [13], respectively.

Figure 2 summarizes the Ce and Fe Néel temperatures of CeFeAs $_{1-x}$ P $_x$ O obtained by measuring the temperature dependence of the Ce magnetic peak $(0, 0, 1)_M$ [13] and Fe $(1, 0, 2)_M$ magnetic scattering. Inspection of the inset of Fig. 2(a) reveals that the Ce long-range ordered moment decreases very rapidly with increasing phosphorus concentration and becomes difficult to detect for $x > 0.25$. The Ce ordering temperatures, however, are only weakly x dependent [Fig. 2(a)]. To quantitatively compare the phosphorus doping dependence of the Fe ordered moment and Néel temperature, we normalized the $(1, 0, 2)_M$ magnetic intensity to the nuclear Bragg peak and plotted their doping and temperature dependence in Figs. 2(b) and 2(c). The Fe ordered moment and ordering temperature gradually decrease with increasing x , and fall below our detection limit of $\sim 0.2 \mu_B/\text{Fe}$ for $x > 0.35$.

To see how phosphorus doping affects the tetragonal to orthorhombic lattice distortion, we plot in Fig. 3 the temperature dependence of the nuclear $(2, 2, 0)_T$ (here the subscript denotes tetragonal structure) peak following previous practice [13]. As the crystal structure changes from

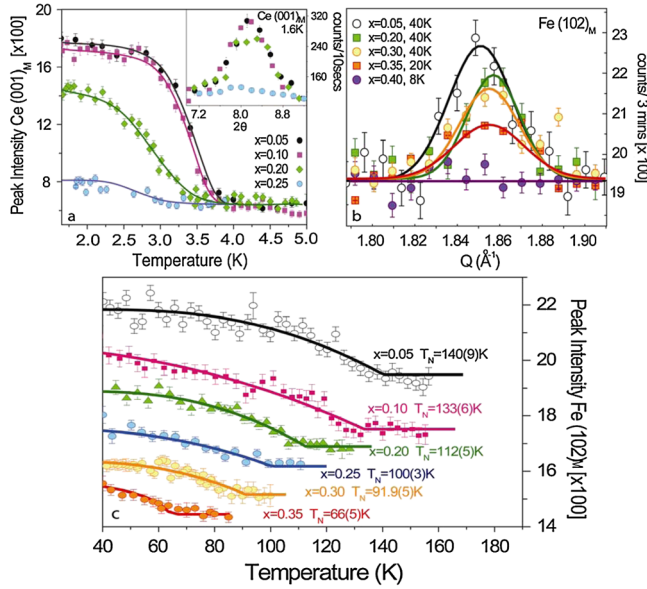


FIG. 2 (color online). (a) Temperature dependence of the Ce $(0, 0, 1)_M$ magnetic Bragg peak for various x . The inset shows the $(0, 0, 1)_M$ peak profile at 1.6 K as a function of x . (b) Doping dependence of the Fe $(1, 0, 2)_M$ magnetic Bragg peak normalized to the nuclear $(1, 1, 1)_O$ peak intensity. The AFM peaks appear at the commensurate ordering wave vectors $Q = 1.851(2), 1.857(2), 1.851(2), 1.855(3), 1.854(4), 1.848(4) \text{ \AA}^{-1}$ for $x = 0.05, 0.10, 0.20, 0.25, 0.30, 0.35, 0.37$, respectively. The corresponding spin-spin correlation lengths are $\xi = 205(24), 179(17), 175(17), 157(23), 174(28), 140(33), 130(29) \text{ \AA}$. The peak positions are essentially doping independent, while the spin-spin correlation length decreases with increasing P concentration. (c) Temperature dependence of the order parameter at the Fe magnetic Bragg peak position $(1, 0, 2)_M$ as a function of P concentration. The Fe ordered moments were estimated from comparing the magnetic scattering intensity with nuclear Bragg intensity at 40 K for $x \leq 0.3$, at 20 K for $x = 0.35$, and at 8 K for $x = 0.37, 0.40, 0.43$. The solid lines are mean field fits to the data.

high temperature tetragonal to the low-temperature orthorhombic phase, the $(2, 2, 0)_T$ peak will split into two peaks [see Figs. 3(a)–3(d)] and a sudden reduction in the scattering intensity at the $(2, 2, 0)_T$ peak position reveals the transition temperature for the lattice distortion [Fig. 3(g)]. With increasing phosphorus concentration, the tetragonal to orthorhombic lattice distortion transition temperature decreases gradually. Although one can still observe a clear kink in temperature dependence of the $(2, 2, 0)_T$ peak intensity near ~ 80 K indicative of the tetragonal to orthorhombic phase transition for $x = 0.3$ (Fig. 3), we were unable to identify the structural phase transition temperatures (if any) for $x > 0.3$. The temperature dependence of the $(2, 2, 0)_T$ peak profile for $x = 0.35$ in Fig. 3(e) confirms the low-temperature phase to be orthorhombic while the tetragonal phase is maintained at all temperatures for $x = 0.40$ as shown in Fig. 3(f).

For a complete determination of the phosphorus doping evolution of the low-temperature crystal structure

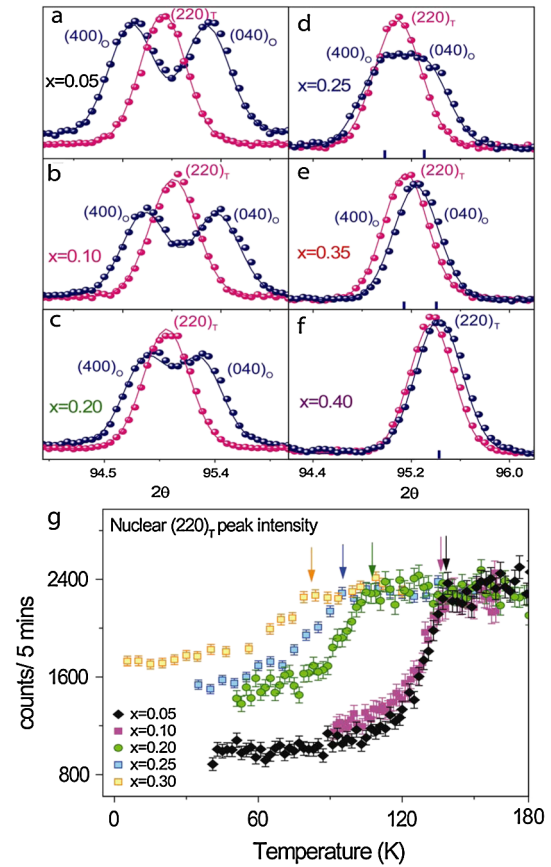


FIG. 3 (color online). (a)–(f) Temperature dependence of the $(2, 2, 0)_T$ (T denotes tetragonal) nuclear reflection at temperatures above and below the structural phase transition for various x . In most cases ($x \leq 0.35$), the low-temperature width is broader than that at high temperatures. (g) Temperature dependence of the $(2, 2, 0)_T$ Bragg peak intensity for different samples, which shows clear kinks indicating tetragonal to orthorhombic phase transitions.

[Fig. 4(a)], we collected full diffraction patterns at low temperatures (see [27] for detailed Rietveld analysis). Figures 4(b)–4(e) summarize the P-doping dependence of the crystal structure in $\text{CeFeAs}_{1-x}\text{P}_x\text{O}$. The undoped CeFeAsO has an orthorhombic low-temperature structure with $c_o > a_o > b_o$ [Fig. 4(b)]. P doping reduces all three lattice parameters with the system becoming tetragonal for $x > 0.37$ [inset in Fig. 4(b)]. The decreased c -axis lattice constant is achieved via a reduction of the As(P)-Fe-As(P) block distance [through reducing the FeAs(P) height when the larger arsenic is replaced by the smaller phosphorus], while the CeAs(P) and CeO block distances remain essentially unchanged with increasing P doping [Fig. 4(d)]. These trends are completely different from that of electron-doped $\text{CeFeAsO}_{1-x}\text{F}_x$, where the c -axis lattice constant contraction is achieved via a large reduction of the Ce-As distance, while the Ce-O(F) and As-Fe-As block distances actually increase with increasing F doping [13]. These fundamental differences reflect the fact that F doping brings the Ce-O(F) charge-transfer layer closer

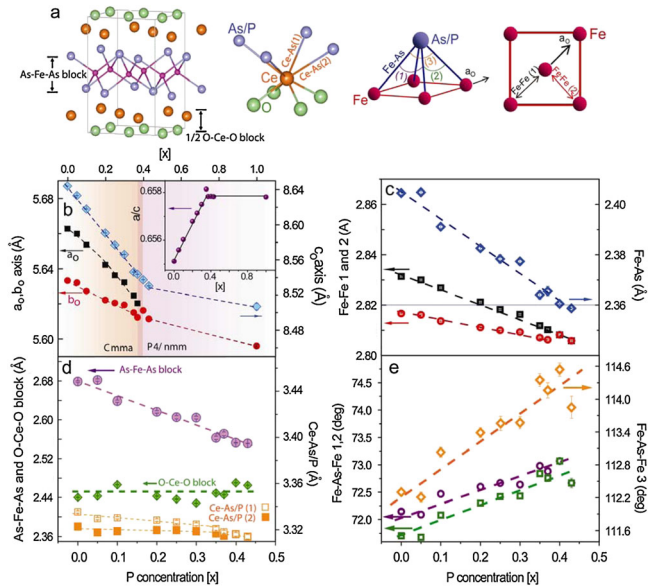


FIG. 4 (color online). (a) schematic diagrams defining the Fe-As-Fe and CeO blocks and illustrating various bond distances and bond angles. (b) a , b , c lattice constants of the orthorhombic unit cell as a function of x . The inset shows that a/c ratio saturates when the Fe moment vanishes. (c) Fe-Fe and Fe-As distances as a function of P concentration. The Fe-As distance falls on the critical value of 2.36 \AA where the Fe ordered moment is suppressed. (d) Ce-O/F and Ce-As distances are essentially P concentration independent. The O-Ce-O block size is also P-substitution independent. The effect of P substitution of As is to reduce the Fe-As bond distance and As-Fe-As block size. This is purely due to the size (lattice) differences between P and As. (e) Fe-As-Fe bond angles as defined in (a) versus P doping. The most dramatic effect of P doping is to increase the Fe-As-Fe angle to 114.6° and decrease the corresponding As-Fe-As angle to 107.3° . Thus, P doping makes the FeAs tetrahedra deviate further from the ideal As-Fe-As angle of 109.5° .

to the superconducting As-Fe-As block and facilitates electron transfer, while P doping is a pure geometrical lattice effect without charge carrier transfer. Furthermore, since the Fe-As distance (2.405 \AA) is essentially doping independent in $\text{CeFeAsO}_{1-x}\text{F}_x$ [13] but decreases rapidly with increasing P doping and saturates at $\sim 2.36 \text{ \AA}$ for $\text{CeFeAs}_{1-x}\text{P}_x\text{O}$ above $x \sim 0.37$ [Fig. 4(c)], the reduced Fe-As(P) distance may induce strong hybridization between the Fe $3d$ and the As $4p$ orbitals and thus quench the ordered Fe magnetic moment in CeFeAsO [28,29].

In summary, we have mapped out the structural and magnetic phase transitions of $\text{CeFeAs}_{1-x}\text{P}_x\text{O}$. We showed that superconductivity does not appear in the magnetic phase diagram over the *entire* measured doping and tem-

perature ranges, thereby establishing that the phosphorous substitution for arsenic in this system is an ideal tuning parameter to explore the magnetic quantum phase transition of the iron pnictides.

The neutron scattering work at UT/ORNL is supported by the DOE BES through DOE DE-FG02-05ER46202, and in part by the DOE BES Division of Scientific User Facilities. The work at the IOP, CAS is supported by the NSFC, the CAS and the MOST. The work at Rice University is supported by the NSF DMR-0706625 and the Robert A. Welch Foundation through C-1411.

*daip@ornl.gov

- [1] Y. Kamihara *et al.*, J. Am. Chem. Soc. **130**, 3296 (2008).
- [2] M. Rotter, M. Tegel, and D. Johrendt, Phys. Rev. Lett. **101**, 107006 (2008).
- [3] X. C. Wang *et al.*, Solid State Commun. **148**, 538 (2008).
- [4] C. de la Cruz *et al.*, Nature (London) **453**, 899 (2008).
- [5] Q. Huang *et al.*, Phys. Rev. Lett. **101**, 257003 (2008).
- [6] S. Li *et al.*, Phys. Rev. B **80**, 020504(R) (2009).
- [7] I. I. Mazin and J. Schmalian, Physica (Amsterdam) **469C**, 614 (2009).
- [8] A. V. Chubukov, Physica (Amsterdam) **469C**, 640 (2009).
- [9] K. Kuroki *et al.*, Phys. Rev. Lett. **101**, 087004 (2008).
- [10] H. Zhai, F. Wang, and D.-H. Lee, Phys. Rev. B **80**, 064517 (2009).
- [11] P. L. Alireza *et al.*, J. Phys. Condens. Matter **21**, 012208 (2009).
- [12] H. Luetkens *et al.*, Nature Mater. **8**, 305 (2009).
- [13] J. Zhao *et al.*, Nature Mater. **7**, 953 (2008).
- [14] A. J. Drew *et al.*, Nature Mater. **8**, 310 (2009).
- [15] G. Aeppli *et al.*, Science **278**, 1432 (1997).
- [16] J. Dai *et al.*, Proc. Natl. Acad. Sci. U.S.A. **106**, 4118 (2009).
- [17] Z. P. Yin *et al.*, Phys. Rev. Lett. **101**, 047001 (2008).
- [18] K. Kuroki *et al.*, Phys. Rev. B **79**, 224511 (2009).
- [19] P. Gegenwart, Q. Si, and F. Steglich, Nature Phys. **4**, 186 (2008).
- [20] S. A. J. Kimber *et al.*, Nature Mater. **8**, 471 (2009).
- [21] F. F. Balakirev *et al.*, Nature (London) **424**, 912 (2003).
- [22] F. Hunte *et al.*, Nature (London) **453**, 903 (2008).
- [23] E. M. Brüning *et al.*, Phys. Rev. Lett. **101**, 117206 (2008).
- [24] Y. K. Luo *et al.*, arXiv:0907.2961.
- [25] G. F. Chen *et al.*, Phys. Rev. Lett. **100**, 247002 (2008).
- [26] A. Jesche *et al.*, Phys. Rev. B **78**, 180504(R) (2008).
- [27] See supplementary material at <http://link.aps.org/supplemental/10.1103/PhysRevLett.104.017204> for experimental details.
- [28] T. M. McQueen *et al.*, Phys. Rev. B **78**, 024521 (2008).
- [29] J. S. Wu, P. Phillips, and A. H. Castro Neto, Phys. Rev. Lett. **101**, 126401 (2008).